

# 1 Non-Steady State Validation of Kinetic Models for Ethylene 2 Epoxidation over Silver Catalysts

3 Lilliana Brandão<sup>1</sup> and Christian Reece<sup>1\*</sup>

4 1. Rowland Institute at Harvard, Harvard University, Cambridge, Massachusetts 02142,  
5 United States

6 \*Corresponding author: [christianreece@fas.harvard.edu](mailto:christianreece@fas.harvard.edu)

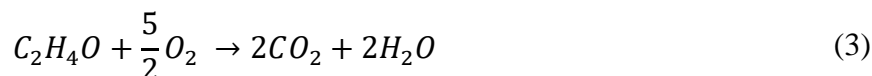
## 7 8 **Abstract**

9  
10 Kinetic modelling has been key to developing a mechanistic understanding of the epoxidation of  
11 ethylene to ethylene oxide over silver catalysts. However, models of varying active site and  
12 mechanistic complexity have all been able to recreate steady state activity and selectivity, leading  
13 to an ambiguity about the exact mechanism and nature of the active site. Herein, we validate three  
14 leading kinetic models for ethylene epoxidation over metallic silver catalysts by numerically  
15 recreating non-steady state Temporal Analysis of Products experiments. We find all of the models  
16 are able to very generally recreate the trends observed in the pulse experiments, but that only a  
17 two-site model modified to mimic the presence of a subsurface oxygen reservoir is able to  
18 accurately recreate the trends observed in a state-altering experiment over oxidised silver. Specific  
19 to this model is the inclusion of a nucleophilic oxygen species adsorbed on top of the surface oxide  
20 which acts as the active site for the selective oxidation of ethylene. This work exemplifies that  
21 while simplified single-site models for ethylene epoxidation are useful tools for broad screening,  
22 more complex models are required to capture the precise activity of the catalyst.

## 23 24 **1. Introduction**

25  
26 Heterogeneous catalytic processes are the driving force of the chemical industry, but their  
27 current use is unsustainable due to environmental, economic, and societal pressures. Despite the  
28 significance of these reactions, industrial innovation has typically outpaced our fundamental  
29 understanding, limiting catalyst development. One such reaction where our application far  
30 outstrips our understanding is the catalytic oxidation of ethylene to ethylene oxide (EO) using  
31 silver catalysts. With its global market value being 54 billion U.S. dollars in 2022, EO is one of  
32 the world's top chemicals.<sup>1</sup> However, despite this widespread use in industry, the underlying  
33 reaction mechanism remains poorly understood.<sup>2</sup>

34  
35 The net reactions for ethylene epoxidation, ethylene combustion, and EO combustion are  
36 as follows:



37 Many studies have sought to resolve the reaction mechanism of ethylene epoxidation over  
38 metallic silver by coupling steady-state activity measurements with kinetic modelling,<sup>3-5</sup> resulting  
39 in a variety of conflicting models. This has led to an open debate not only on the reaction  
40 mechanism, but also on the identity of the active site for this reaction.<sup>2,6-9</sup> For ethylene epoxidation  
41 over silver there are three popular microkinetic models: The Linic-Barteau (LB) model was  
42 developed using Density Functional Theory (DFT) and surface science experiments to generate a  
43 simple 4-step, single site microkinetic model that was able to recreate the apparent activation  
44 energy of EO production.<sup>3</sup> The Huš-Hellman (HH) model used DFT to generate an 11-step, single  
45 site microkinetic model that was validated by comparing kinetic Monte Carlo simulations to  
46 experimentally measured turnover frequencies and selectivities.<sup>4</sup> Finally, the Stegelemann-Stoltze  
47 (SS) model used a combination of DFT and surface science to generate a 17-step, two-site  
48 microkinetic model that was able to recreate experimental turnover frequencies and selectivities  
49 across a wide range of conditions.<sup>5,10</sup> As these models are validated against steady-state  
50 experiments, the number of activity or selectivity controlling reaction steps collapses down to a  
51 small (or single) number,<sup>11</sup> which limits kinetic insight and can be the cause of the degeneracy  
52 seen in the models. Further, if we are to move beyond broad screening of reaction conditions to  
53 resolving the precise refinements required to increase catalytic activity and selectivity, more  
54 accurate models are required. Therefore, an external method of validating existing kinetic models  
55 against independent data recorded under different reaction conditions can provide insight into the  
56 broad applicability of these models, which, in turn, will help identify the reaction mechanism.

57  
58 Non-steady-state techniques such as Temporal Analysis of Products<sup>12,13</sup> (TAP) bypass the  
59 steady-state limitations, providing precisely resolved kinetic information and allowing more  
60 complex kinetic features to be evolved during the experiment. Previous experiments studying the  
61 epoxidation of ethylene over a metallic silver powder have been examined using TAP,<sup>14</sup> providing  
62 some mechanistic insight, but no kinetic modelling of the TAP experiments was performed. The  
63 microkinetic modelling of TAP experiments is well-established<sup>15-17</sup> but is seldom utilised for  
64 multi-step reactions due to the significant computational cost of the numerical simulations. Herein,  
65 we have developed a purpose-built TAP simulation package, SimTAP, that can rapidly simulate  
66 complex multi-step reaction networks. For the first time, we are able to precisely recreate entire

67 TAP experiments, affording simulation of hundreds of pulses, and allowing the catalyst surface to  
68 evolve dynamically during the simulation as it would during the experiments.

69  
70 In this work we have validated the LB, HH, and SS kinetic models against a series of TAP  
71 experiments performed over a metallic silver catalyst.<sup>14</sup> We find that all the models were able to  
72 qualitatively recreate a single-pulse and one of the pump-probe TAP experiments over a metallic  
73 silver surface, with the HH model being the most accurate. However, more complex oxidation-  
74 titration experiments where the metallic silver catalyst is oxidised by pulsing O<sub>2</sub> and then  
75 subsequently reduced by pulsing ethylene were poorly reproduced. By adjusting the HH model  
76 to approximate the role of lateral interactions, we found that it was able to partially recreate the  
77 observed trends in the production of EO, but not CO<sub>2</sub>. We have found that by modifying the SS  
78 model to stop the decomposition of the oxide, and with slight changes to the physical  
79 characteristics of the TAP experiment, the qualitative trends in EO and CO<sub>2</sub> production were  
80 reproduced. We find that while single-site models are applicable for broad screening of general  
81 catalytic activity, more complex models involving lateral interactions or multiple active sites are  
82 required to precisely recreate the observed activity and selectivity trends.

83

## 84 2. Materials and Methods

85

86 **2.1 TAP simulations.** The modelling of TAP experiments has been described extensively in the  
87 literature,<sup>12,15,18–20</sup> but it is repeated here for clarity. The TAP reactor is partitioned into zones,  
88 with the typical setup consisting of three zones that contain inert packing, catalyst, and inert  
89 packing respectively,<sup>19</sup> but TAP reactors consisting of a single catalyst zone are also utilised.<sup>14</sup>  
90 The transport of a reversibly adsorbing gas A through a zone during a TAP experiment is described  
91 using the following system of differential equations:

$$\varepsilon_b \frac{\partial C_A}{\partial t} = D_{eA} \frac{\partial^2 C_A}{\partial z^2} - S_V(1 - \varepsilon_b)(k_a C_A \theta_* - k_d \theta_A) \quad (4)$$

92 where  $\varepsilon_b$  is the void fraction of the reactor,  $C_A$  is the concentration of species A (mols/cm<sup>3</sup>),  $t$  is  
93 the time (s),  $D_{eA}$  is the effective Knudsen diffusivity of gas A (cm<sup>2</sup>/s),  $z$  is the axial coordinate of  
94 the reactor (cm),  $S_V$  is the surface area of catalyst per volume of catalyst (cm<sup>2</sup>/cm<sup>3</sup>),  $k_a$  is the  
95 adsorption rate constant (cm<sup>3</sup>/mols/s),  $\theta_*$  is the concentration of free sites (mols/cm<sup>2</sup>),  $k_d$  is the  
96 desorption rate constant (s<sup>-1</sup>), and  $\theta_A$  is the concentration of adsorbed A (mols/cm<sup>2</sup>). The surface  
97 species are modelled using a mean-field microkinetic model, which for a reversibly adsorbing  
98 species would be:

$$\frac{\partial \theta_A}{\partial t} = k_a C_A \theta_* - k_d \theta_A \quad (5)$$

99 For noninteracting cases (such as in the inert zones) the terms  $k_a$  and  $k_d$  can be set to zero leaving:

$$\varepsilon_b \frac{\partial C_A}{\partial t} = D_{eA} \frac{\partial^2 C_A}{\partial z^2} \quad (6)$$

100 For a gas being pulsed into the reactor the initial condition is defined as:

$$C_A(z, 0) = \delta(z, 0) \quad (7)$$

101 where  $\delta(z, 0)$  represents a delta function introduced into the reactor at a time  $t = 0$ . After  
102 introducing the pulse into the microreactor, the pulse valve is closed, and so the boundary at the  
103 reactor exit can be defined as:

$$\frac{\partial C_A(0, t)}{\partial z} = 0 \quad (8)$$

104 As the exit of the microreactor is attached to a vacuum, the exit condition is defined as:

$$C_A(L, t) = 0 \quad (9)$$

105 where  $L$  is the total length of the reactor (cm). Finally, the flux of gas leaving the reactor, which is  
106 recorded during the experiment, is defined as:

$$F_A = -D_{eA} \frac{\partial C_A(L, t)}{\partial z} \quad (10)$$

107 where  $F_A$  is the flux of gas A leaving the reactor (mols/cm<sup>3</sup>/s). For simple cases where the kinetics  
108 can be approximated to first-order, or where there are no kinetics (diffusion only) generalised  
109 analytical solutions exist for any number of zones and configurations.<sup>18,21</sup> For more complex  
110 kinetics (e.g., second order), such as those used in this paper, the TAP experiment must be  
111 numerically simulated. To numerically simulate the TAP experiment, the series of partial  
112 differential equations must be converted to a series of ordinary differential equations using a finite-  
113 element method which can then be evaluated using standard ODE solvers. An excellent description  
114 of how the method of lines can be applied to this series of equations is described in the previous  
115 literature.<sup>15</sup>

116  
117 To perform the numerical simulation of the various TAP experiments outlined in this paper,  
118 a generalised TAP simulation package (SimTAP) was developed in the MATLAB environment.  
119 Similar to the previously published Python package TAPSolver<sup>17</sup> and the FORTRAN code  
120 TAPFIT,<sup>22</sup> SimTAP reads in a user generated input file describing the simulation parameters (e.g.,  
121 kinetic model, kinetics, temperature, reactor length, simulation time) and numerically simulates  
122 the corresponding TAP experiment. Using the method of lines,<sup>15</sup> the series of partial differential

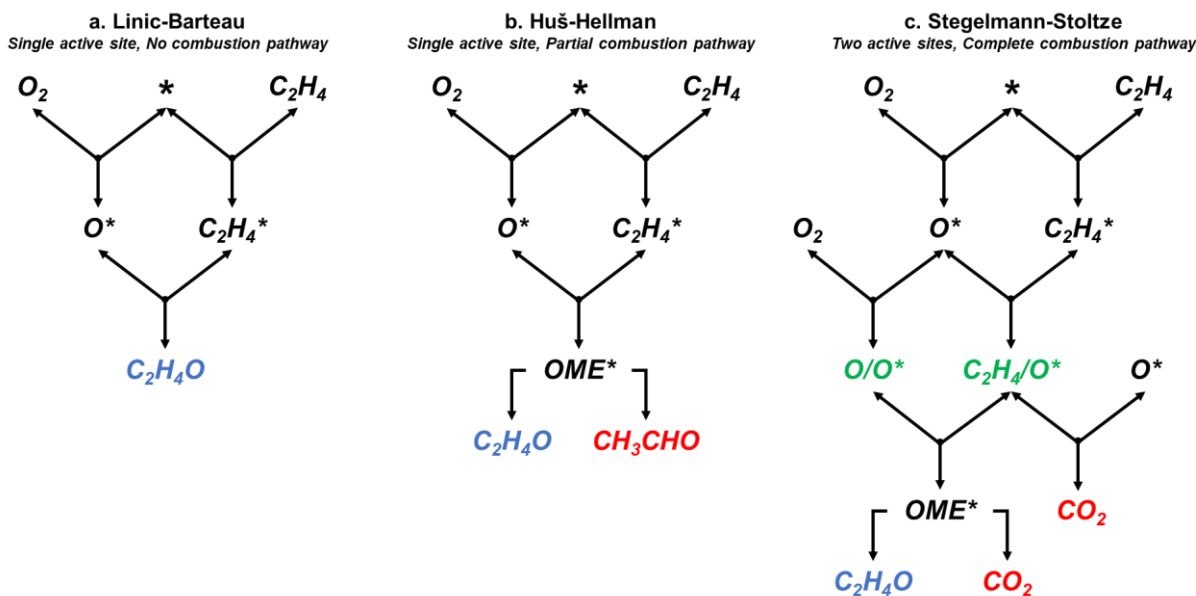
123 equations are transformed to a series of ordinary differential equations and numerically integrated  
124 using MATLAB's in-built ODE15s solver. Differing from the previous packages (TAPSolver,  
125 TAPFIT) which primarily focus on the fitting and analysis of experimental data, the SimTAP  
126 package is highly optimised to simulate complex multi-step TAP experiments. When performing  
127 a single pulse experiment, the initial concentration of surface species and size of the pulse are set  
128 using the input file. When performing multi-pulse experiments, during which both gas and surface  
129 species build up, the SimTAP package takes the exit condition from the previous pulse simulation  
130 and uses it as the initial condition for the next pulse simulation, with another pulse generated by  
131 addition of a delta function. The initial concentrations of gas and surface species during a multi-  
132 pulse experiment are set using:

$$C_A^{N+1}(z, 0) = C_A^N(z, t_{max}) + \delta(z, 0) \quad (11)$$

$$\theta_A^{N+1}(z, 0) = \theta_A^N(z, t_{max}) \quad (12)$$

133 where  $N$  is the current pulse number and  $t_{max}$  is the total simulation time. For pump-probe  
134 experiments, the simulation time ( $t_{max}$ ) is set to the duration of the “pump” pulse, and the  
135 simulation is repeated with a new inlet species as the “probe” pulse. A beta version of the package  
136 is provided with the supplementary material, alongside the input files utilised in this work.

137  
138 **2.2 Adaptation of kinetic models.** To adapt the kinetic models for use in the TAP simulations,  
139 the activation energies and pre-exponential factors were adjusted to obtain consistent units as  
140 required by SimTAP. The activation energies for each step were converted to units of kJ/mol, and  
141 the pre-exponential factors were converted to  $s^{-1}$  for first order reactions,  $cm^2s^{-1}$  for second order  
142 surface reactions, and  $cm^3s^{-1}$  for adsorption steps. The three microkinetic models and adjusted  
143 Arrhenius parameters at 570 K are shown in table 1 and are summarised graphically in Figure 1.



144  
 145 **Figure 1.** Simplified representations of the (a) Linic-Barteau,<sup>3</sup> (b) Huš-Hellman,<sup>4</sup> and (c)  
 146 Stegelemann-Stoltze reaction networks.<sup>5</sup> \* indicates empty metallic site. X\* indicating an adsorbed  
 147 species. OME denotes the oxametallacycle intermediate. /O\* indicates a species adsorbed on an  
 148 oxide site.

149  
 150 The three models have varying characteristics and levels of complexity. The LB model  
 151 includes four reversible steps and a single active site. It assumes the formation of EO occurs  
 152 through an oxametallacycle (OME) intermediate that is not explicitly modelled, and does not  
 153 include a combustion pathway (Figure 1a).<sup>3</sup> The HH model includes 11 reversible steps and has a  
 154 single active site which forms an explicitly modelled OME intermediate that can either form EO  
 155 or decomposes to acetaldehyde (Figure 1b). As acetaldehyde would rapidly decompose to CO<sub>2</sub>  
 156 under the experimental conditions,<sup>23</sup> it was assumed to be qualitatively analogous to CO<sub>2</sub>  
 157 production for comparison purposes. The SS model includes 17 reversible steps, two of which (10  
 158 reverse and 4 reverse) have very high activation barriers and were removed by setting their pre-  
 159 exponential factors to zero to speed up the simulations. The SS model contains two active sites; in  
 160 addition to the metallic silver site (\*) it includes a surface oxide active site, denoted by /O\*. In this  
 161 model it is the reaction between C<sub>2</sub>H<sub>4</sub> adsorbed at an oxide site (C<sub>2</sub>H<sub>4</sub>/O\*) and a nucleophilic  
 162 oxygen species adsorbed on top of a surface oxide (O/O\*) that forms the OME intermediate (Figure  
 163 1c). This model also includes a full combustion pathway of the OME intermediate and adsorbed  
 164 C<sub>2</sub>H<sub>4</sub> resulting in the production of CO<sub>2</sub> and H<sub>2</sub>O.<sup>5</sup>

165  
 166 For the LB and SS models, the pre-exponential factors provided were adjusted as follows  
 167 for implementation in SimTAP. For first order surface and desorption steps no adjustment was  
 168 necessary because the factors were already reported in s<sup>-1</sup>. For second order surface steps the pre-  
 169 exponential factors were adjusted by dividing the reported values by the catalyst site density to

170 achieve units of  $\text{cm}^2\text{s}^{-1}$ . For adsorption steps, the initial sticking coefficient was calculating using  
171 the following equation:<sup>5</sup>

$$s^0 = \frac{kP}{d\sqrt{2\pi mk_B T}} \quad (13)$$

172  
173 Where  $s^0$  is the calculated initial sticking rate,  $k$  is the reported rate constant for adsorption ( $\text{s}^{-1}$ ),  
174  $P$  is the thermodynamic reference pressure (Pa),  $d$  is the density of sites ( $\text{sites}/\text{m}^2$ ),  $m$  is mass of  
175 the gas molecule (kg),  $k_B$  is the Boltzmann constant, and  $T$  is temperature (K) at which the pre-  
176 exponential factors were calculated at in each respective model. For the LB model,  $P$  was 101325  
177 Pa,  $d$  was  $1 \times 10^{19}$   $\text{sites}/\text{m}^2$  (approximated as the surface site density in the original TAP study<sup>14</sup>),  
178 and  $T$  was 298 K. For the SS model,  $P$  was  $1 \times 10^5$  Pa,  $d$  was  $6.9 \times 10^{18}$   $\text{sites}/\text{m}^2$ , and  $T$  was 500 K.

179  
180 Pre-exponential factors for adsorption steps were subsequently calculated in units of  $\text{cm}^3\text{s}^{-1}$   
181 using the following equation:<sup>24</sup>

$$k_a = \frac{s^0}{\sigma} \sqrt{\frac{RT}{2\pi M}} \quad (14)$$

182 where  $k_a$  is the pre-exponential factor for adsorption ( $\text{m}^3\text{s}^{-1}$ ),  $\sigma$  is the surface site density ( $\text{sites}/\text{m}^2$ )  
183 in the experimental setup,  $R$  is the ideal gas constant,  $T$  is experiment temperature (K), and  $M$  is  
184 molecular weight (kg/mol). In the LB and SS models, parameters were reported for temperatures  
185 of 298 K and 500 K respectively. Pre-exponential factors for adsorption steps were scaled to  
186 accommodate for temperature differences across the experiments, however, we assumed  
187 temperature scaling to not be significant under the simulation conditions for other parameters.

188  
189 For the HH model the activation energies were taken from those calculated on the Ag(111)  
190 surface because it is the most stable facet and most common in untreated catalysts. The Ag(111)  
191 surface was also found to show the best agreement with bulk experimental data.<sup>4</sup> The HH model  
192 did not provide pre-exponential factors, so those values were approximated using transition state  
193 theory.<sup>25</sup> Pre-exponential factors were estimated to be  $1 \times 10^{13} \text{ s}^{-1}$  for first order surface steps,  $1 \times 10^7$   
194  $\text{cm}^2\text{s}^{-1}$  for fast second order surface reaction steps (*i.e.*, the formation/decomposition of OME\*),  
195  $1 \times 10^7 \text{ cm}^2\text{s}^{-1}$  for slow second order surface reaction steps (*i.e.*, decomposition of surface oxygen  
196 species), and  $1 \times 10^{15} \text{ s}^{-1}$  for first order desorption steps. For adsorption steps, pre-exponential  
197 factors were estimated and scaled using equation 14. The initial sticking rate ( $s^0$ ) was assumed to  
198 be 1 for all gases. Further, the oxygen diffusion step from the original HH model is not included  
199 as it is not relevant for a mean-field simulation.

200  
201  
202

203 **Table 1.** Kinetic model steps, pre-exponential factors (A), and activation energies ( $E_a$ ) for the  
 204 Linc-Bartreau (LB),<sup>3</sup> Huš-Hellman (HH),<sup>4</sup> and Stegelmann-Stoltze (SS)<sup>5</sup> models at 570 K. Pre-  
 205 exponential factors (A) are shown for a temperature of 570 K and have been scaled. Pre-  
 206 exponential factors are listed in units of  $s^{-1}$  for first order steps,  $cm^2s^{-1}$  for second order surface  
 207 steps, and  $cm^3s^{-1}$  for second order adsorption steps. In the HH model, steps 3 reverse and 4 reverse  
 208 were estimated as slow second order surface steps, while steps 5 forward and 5 reverse were  
 209 estimated as fast second order surface steps. OME represents the oxametallacycle intermediate. In  
 210 the HH model steps 2 forward and 4 forward and in the SS model steps 3 forward, 10 forward, and  
 211 14 forward were considered pseudo-second order. Steps 10 reverse and 14 reverse in the SS model  
 212 were turned off in the simulations by setting their pre-exponential factors to zero due to their large  
 213 activation energies.

#### Linc-Bartreau<sup>3</sup>

Number	Step	$A_{fwd}$	$E_{a,fwd}$ (kJ/mol)	$A_{rev}$	$E_{a,rev}$ (kJ/mol)
1	$O_2 + 2^* \rightleftharpoons 2O^*$	$2.8 \times 10^{-13}$	72.4	$4.0 \times 10^{-2}$	135.1
2	$C_2H_4 + ^* \rightleftharpoons C_2H_4^*$	$5.6 \times 10^{-14}$	0.0	$1.0 \times 10^{13}$	33.5
3	$O^* + C_2H_4^* \rightleftharpoons C_2H_4O^* + ^*$	$2.0 \times 10^{-4}$	62.3	$1.0 \times 10^{-2}$	100.4
4	$C_2H_4O^* \rightleftharpoons C_2H_4O + ^*$	$4.0 \times 10^{13}$	66.9	$4.5 \times 10^{-12}$	46.0

#### Huš-Hellman<sup>4</sup>

Number	Step	$A_{fwd}$	$E_{a,fwd}$ (kJ/mol)	$A_{rev}$	$E_{a,rev}$ (kJ/mol)
1	$C_2H_4 + ^* \rightleftharpoons C_2H_4^*$	$1.6 \times 10^{-11}$	0.0	$1.0 \times 10^{15}$	7.7
2	$O_2 + 2^* \rightleftharpoons O_2^{**}$	$1.5 \times 10^{-11}$	0.0	$1.0 \times 10^{15}$	18.3
3	$O_2^{**} \rightleftharpoons 2O^*$	$1.0 \times 10^{13}$	80.1	$1.0 \times 10^{-7}$	126.4
4	$O_2 + 2^* \rightleftharpoons 2O^*$	$1.5 \times 10^{-11}$	61.8	$1.0 \times 10^{-7}$	126.4
5	$C_2H_4^* + O^* \rightleftharpoons OME^* + ^*$	$1.0 \times 10^{-2}$	45.4	$1.0 \times 10^{-2}$	63.7
6	$C_2H_4 + O^* \rightleftharpoons OME^*$	$1.6 \times 10^{-11}$	28.9	$1.0 \times 10^{15}$	63.7
7	$OME^* \rightleftharpoons C_2H_4O^*$	$1.0 \times 10^{13}$	71.4	$1.0 \times 10^{13}$	93.6
8	$OME^* \rightleftharpoons CH_3CHO^*$	$1.0 \times 10^{13}$	65.6	$1.0 \times 10^{13}$	189.1
9	$C_2H_4O^* \rightleftharpoons C_2H_4O + ^*$	$1.0 \times 10^{15}$	9.6	$1.3 \times 10^{-11}$	0.0
10	$CH_3CHO^* \rightleftharpoons CH_3CHO + ^*$	$1.0 \times 10^{15}$	3.9	$1.3 \times 10^{-11}$	0.0

#### Stegelmann-Stoltze<sup>5</sup>

Number	Step	$A_{fwd}$	$E_{a,fwd}$ (kJ/mol)	$A_{rev}$	$E_{a,rev}$ (kJ/mol)
1	$O_2 + ^* \rightleftharpoons O_2^*$	$1.4 \times 10^{-14}$	5.7	$1.1 \times 10^{12}$	47.3
2	$O_2^* + ^* \rightleftharpoons 2O^*$	$4.0 \times 10^{-3}$	75.0	$8.0 \times 10^{-1}$	157.5
3	$O_2 + 2O^* \rightleftharpoons 2O/O^*$	$1.0 \times 10^{-12}$	20.0	$1.3 \times 10^0$	96.9
4	$C_2H_4 + O^* \rightleftharpoons C_2H_4/O^*$	$3.7 \times 10^{-12}$	0.0	$2.2 \times 10^{11}$	37.1
5	$C_2H_4/O^* + O/O^* \rightleftharpoons OME^* + O^*$	$9.0 \times 10^{-1}$	112.0	$5.3 \times 10^{-1}$	183.3
6	$C_2H_4O + O^* \rightleftharpoons C_2H_4O/O^*$	$9.9 \times 10^{-12}$	0.0	$4.8 \times 10^{12}$	39.1
7	$OME^* \rightleftharpoons C_2H_4O/O^*$	$1.1 \times 10^{13}$	95.0	$2.1 \times 10^{12}$	93.5
8	$OME^* \rightleftharpoons CH_3CHO/O^*$	$9.0 \times 10^{12}$	95.0	$4.5 \times 10^{10}$	204.3
9	$CH_3CHO/O^* \rightleftharpoons CH_3CHO + O^*$	$2.9 \times 10^{13}$	41.9	$1.3 \times 10^{-10}$	4.4

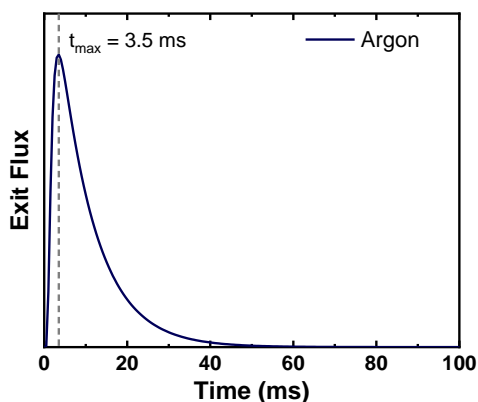


10	$\text{CH}_3\text{CHO}/\text{O}^* + 6\text{O}^*$	$\rightleftharpoons$	$2\text{CO}_2^* + 4\text{OH}^* + ^*$	$2.0 \times 10^5$	11.0	-	-
11	$\text{C}_2\text{H}_4 + ^*$	$\rightleftharpoons$	$\text{C}_2\text{H}_4^*$	$3.7 \times 10^{-12}$	0.0	$2.2 \times 10^{11}$	30.1
12	$\text{C}_2\text{H}_4/\text{O}^* + \text{O}^*$	$\rightleftharpoons$	$\text{C}_2\text{CHOH}/\text{O}^* + ^*$	$4.0 \times 10^{-4}$	32.0	$3.1 \times 10^{-1}$	42.8
13	$\text{CH}_2\text{CHOH}/\text{O}^* + \text{O}^*$	$\rightleftharpoons$	$\text{CH}_2\text{CHO}/\text{O}^* + \text{OH}^*$	$2.6 \times 10^{-2}$	86.0	$1.3 \times 10^{-6}$	106.1
14	$\text{CH}_2\text{CHO}/\text{O}^* + 5\text{O}^*$	$\rightleftharpoons$	$2\text{CO}_2^* + 3\text{OH}^* + ^*$	$1.0 \times 10^5$	0.0	-	-
15	$2\text{OH}^*$	$\rightleftharpoons$	$\text{H}_2\text{O}^* + \text{O}^*$	$1.4 \times 10^{-5}$	65.6	$1.0 \times 10^{-4}$	50.0
16	$\text{CO}_2^*$	$\rightleftharpoons$	$\text{CO}_2 + ^*$	$3.6 \times 10^{14}$	38.9	$5.1 \times 10^{-12}$	0.0
17	$\text{H}_2\text{O}^*$	$\rightleftharpoons$	$\text{H}_2\text{O} + ^*$	$5.9 \times 10^{14}$	46.6	$7.1 \times 10^{-11}$	0.0

214 Metallic silver sites are denoted by  $^*$ . Surface oxide sites are denoted by  $/\text{O}^*$ . Species adsorbed on  
 215 metallic silver and surface oxide sites are denoted by  $\text{X}^*$  and  $\text{X}/\text{O}^*$ , respectively.

216

217 **2.3 Implementation of reactor and experimental parameters.** Reactor parameters were set to  
 218 match those reported in the original TAP study.<sup>14</sup> The microreactor was 1.25 cm long with a  
 219 diameter of 0.64 cm. The catalyst was 500 mg of silver powder with an estimated active site density  
 220 of  $1 \times 10^{15}$  sites per  $\text{cm}^2$ . The catalyst surface area was  $800 \text{ cm}^2 \text{ g}^{-1}$ . We estimated a standard value  
 221 of 0.4 for voidage in the silver catalyst zone. The diffusivity of Ar through the reactor at 298 K  
 222 was estimated to be  $35 \text{ cm}^2 \text{ s}^{-1}$ , based on the reported time of maximum intensity of Ar at 570 K in  
 223 the original study (Figure 2).<sup>14</sup> The pulse size was  $1 \times 10^{17}$  molecules per pulse unless otherwise  
 224 noted. These parameters were kept consistent across all models and simulations.



225  
 226 **Figure 2.** Simulated pulse of Ar through the TAP microreactor with the time of maximum intensity  
 227 overlaid. The maximum intensity matches that reported experimentally of 3.5 ms.<sup>14</sup>

228

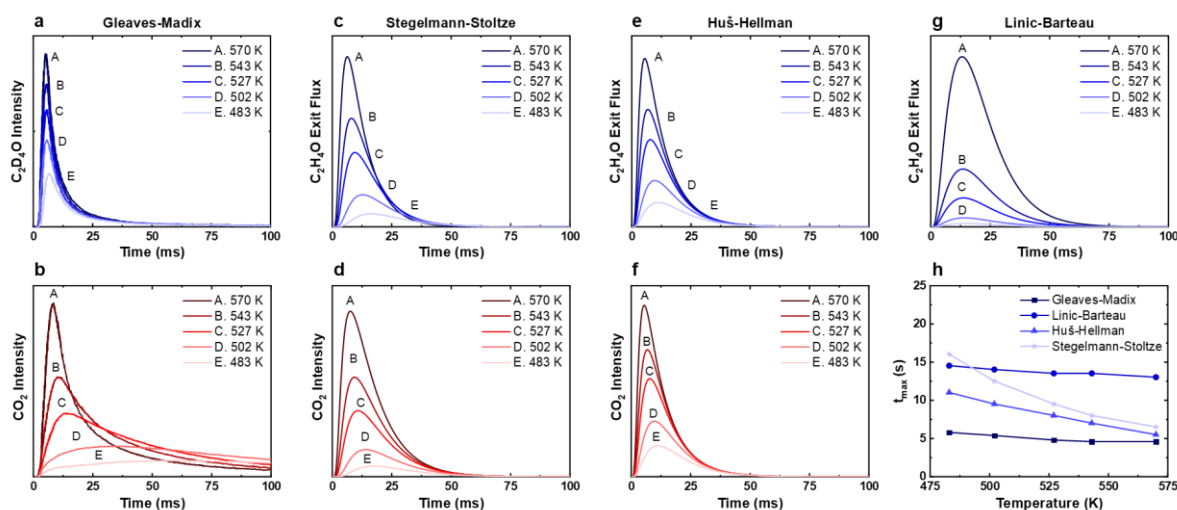
### 229 3. Results

230

231 A total of four TAP experiments were implemented in SimTAP to validate the models.  
 232 One single-pulse, two pump-probe, and one multi-pulse oxidation-titration experiment.  
 233 Simulations of these four experiments utilised the physical parameters exactly as reported in the  
 234 ethylene oxidation TAP study<sup>14</sup> and the kinetic parameters as adapted from the three microkinetic  
 235 models.<sup>3-5</sup> In the experiments, deuterated ethylene was used due to the overlapping masses of EO  
 236 and  $\text{CO}_2$ , however in the simulation this is not required. Any kinetic isotope effect that arises from  
 237 deuterated ethylene is considered negligible for the purposes of comparison.

238  
239  
240  
241  
242  
243  
244  
245  
246  
247  
248  
249

**3.1 Single-pulse experiments.** In the single-pulse TAP experiment, O<sub>2</sub> and ethylene were pulsed together in a one-to-one ratio ( $1 \times 10^{17}$  molecules of each gas per pulse) over the clean (metallic) silver catalyst at temperatures ranging from 483 – 570 K (Figure 3) to probe the temperature dependence of the EO reaction over metallic silver. The products were measured for a total of 200 ms from the initiation of the O<sub>2</sub> and ethylene pulse. Four main features were observed in the experiment: First, the conversion of ethylene was recorded to be ~1% at 570 K. Second, increasing the temperature increased the amount of EO produced (Figure 3a). Third, increasing the temperature increased the amount of CO<sub>2</sub> produced. Finally, the time of peak EO production was observed to occur earlier with increasing temperature, with time of peak production ranging from 5.8 ms at 483 K to 4.6 ms at 570 K (Figure 3h).



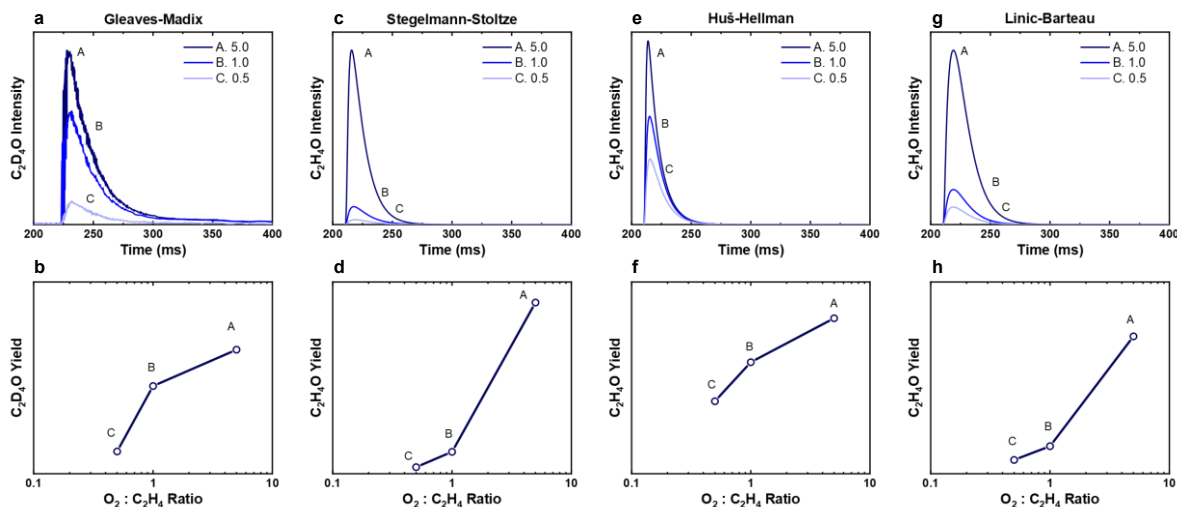
250  
251 **Figure 3.** (a-b) Experimental and (c-g) simulated exit flux curves for the single-pulse experiment  
252 where ethylene and O<sub>2</sub> were pulsed over the clean catalyst at varying temperatures from 483 – 570  
253 K. (h) Experimental and simulated time of maximum ethylene oxide production ( $t_{\max}$ ) as a function  
254 of temperature. All three simulated models show qualitative agreement with the experimentally  
255 measured results. Experimental data was adapted from ref.<sup>14</sup>  
256

257 In the simulations, the conversion of ethylene at 570 K was calculated to be 0.04% for the  
258 LB model, 77.9% for the HH model, and 20.9% for the SS model, showing poor quantitative  
259 agreement with the experimentally measured 1% conversion. This is expected as kinetic models  
260 are typically validated against experimental turnover frequencies on a logarithmic scale, as such,  
261 only qualitative comparisons will be made from here on out. All three models recreate the trend of  
262 increasing EO production with increasing temperature (Figures 3c, 3e, and 3g). Additionally, all  
263 three models show relatively consistent EO response shapes across the different temperatures,  
264 although the shape of the EO responses in the LB model were noticeably broader than those  
265 measured experimentally. This demonstrates that all three models are able to recreate the  
266 temperature dependence of the reaction over metallic silver, which is not surprising given that they

267 are validated against steady-state data recorded at varying temperatures. The CO<sub>2</sub> and acetaldehyde  
268 pulse responses for the SS (Figure 3d) and HH (Figure 3f) models respectively also matched the  
269 experimental trend of increased production with increasing temperature. However, both the SS  
270 and HH model simulations were not able to recreate the significant broadening observed in the  
271 CO<sub>2</sub> response shape at lower temperatures. Some minor broadening was seen in the SS responses  
272 at lower temperatures, but not comparable to the amount seen experimentally. Given the significant  
273 complexity of combustion pathways, it is expected that the rate of CO<sub>2</sub> production cannot be  
274 described by a simple second order reaction as is utilised in the models (Table 1) and indicates that  
275 further refinement of these pathways may be necessary. As the LB model does not include a  
276 combustion pathway, no comparison could be made. All three models showed a negative slope  
277 when time of maximum intensity of EO as a function of temperature was graphed, however, the  
278 time values were consistently higher in the simulated results. In summary, the single-pulse  
279 experiments show that all three models are able to generally predict the behaviour observed in the  
280 TAP experiments.

281  
282 **3.2 Pump-probe experiments.** Two pump-probe experiments were performed over the metallic  
283 silver catalyst. In the first experiment, a pulse of O<sub>2</sub> was applied to a cleaned catalyst surface (the  
284 “pump”), and then after a time delay of 210 ms, ethylene was pulsed (the “probe”) at varying ratios  
285 of O<sub>2</sub> to ethylene at a temperature of 523 K. The amount of ethylene was kept constant at  $1 \times 10^{17}$   
286 molecules per pulse, and the amount of O<sub>2</sub> was varied to maintain ratios of 5, 1, and 0.5 parts O<sub>2</sub>  
287 to 1 part ethylene. By varying the size of the oxygen pump response, different coverages of oxygen  
288 on the surface are attained, allowing the relationship between EO production and surface oxygen  
289 coverage to be probed. However, the absolute coverage of the surface oxygen species remains  
290 sufficiently low such that during the experiment the silver remains metallic. The experimental  
291 results showed an approximately linear increase in EO production with increasing O<sub>2</sub> to ethylene  
292 ratio (Figure 4a).<sup>14</sup>

293  
294 The simulated results for all three models all recreated the trend of increasing EO  
295 production with increased O<sub>2</sub> to ethylene ratio (Figures 4b, 4c, 4d). The LB and SS model  
296 simulated results showed poor qualitative agreement, as the difference in the amount of EO  
297 produced between ratios 1 and 5 was significantly higher in the models than in the experiment,  
298 showing an almost exponential increase in EO production with increasing surface coverage. In  
299 comparison, the HH model showed better qualitative agreement with the experimental results,  
300 showing a more linear relationship in EO production with increasing surface coverage. This  
301 demonstrates that over metallic surfaces, a single-site model is sufficient to capture the relationship  
302 between ethylene oxide production and surface oxide coverage, and that the coverage dependence  
303 of the two-site model may not be correct over a metallic surface.  
304

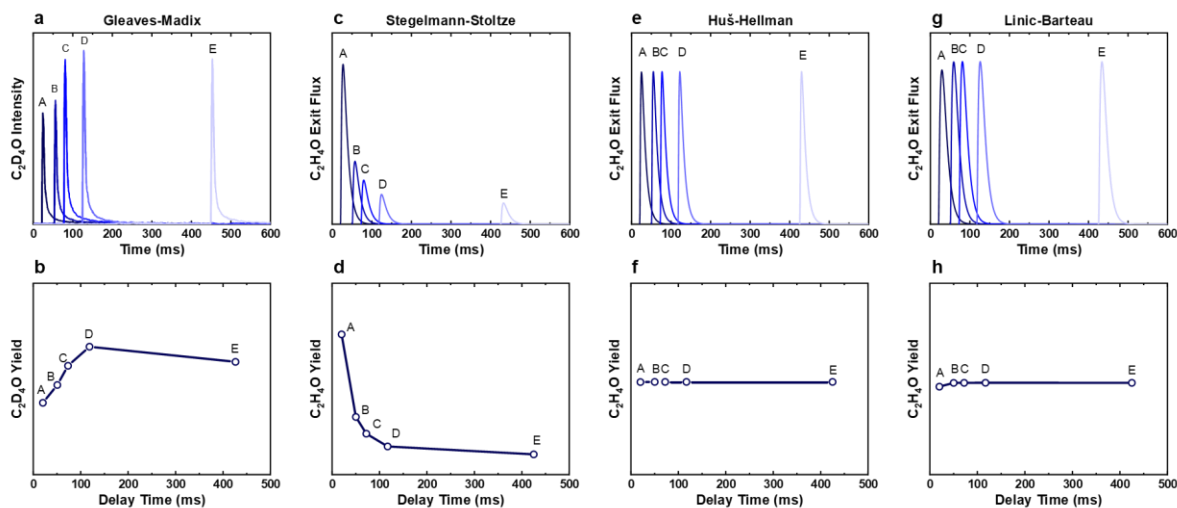


305  
 306 **Figure 4.** (a-b) Experimental and (c-h) simulated ethylene oxide responses and yields for pump-  
 307 probe experiments with varied oxygen to ethylene ratios at 523 K. The experimental results  
 308 showed increased ethylene oxide production with increasing oxygen to ethylene ratio<sup>14</sup> with the  
 309 simulated results showing similar general trends, but the HH model is the only one to have a  
 310 concave type relationship with increasing O<sub>2</sub>:C<sub>2</sub>H<sub>4</sub> ratio. Experimental data was adapted from  
 311 ref.<sup>14</sup>

312 In the second pump-probe experiment, the ratio of O<sub>2</sub> to ethylene was held constant at 1:1,  
 313 and the time interval between the pump and probe pulse was varied at a temperature of 523 K. The  
 314 time intervals used were 20, 50, 72, 117, and 425 ms. As the surface oxide is expected to  
 315 decompose as a function of time, this experiment probes the rate of surface oxygen decomposition  
 316 as a function of time and the relationship between surface oxide coverage and EO production  
 317 simultaneously. Further, similar to the previous experiment, the absolute coverage of the surface  
 318 oxide is sufficiently low that the catalyst remains metallic. Experimentally it was found that the  
 319 peak EO production was at a 117 ms interval (Figure 5a, 5b), almost double the amount measured  
 320 at a 20 ms interval. A small drop in EO production was also recorded at an interval of 425 ms, but  
 321 EO was still produced at higher yields than at time delays of less than the peak at 117 ms. This  
 322 experiment indicated that the relationship between surface oxide coverage and EO production was  
 323 more complex than a simple linear relationship, and the lifetime of the surface oxide is longer than  
 324 the ~400ms probed.

325  
 326 None of the models were found to recreate the experimentally observed trend. The SS  
 327 model showed peak production of EO in the shortest time delay of 20 ms, with rapidly decreasing  
 328 production with increasing time delay and almost no production of EO recorded at a delay of 425  
 329 ms (Figure 5c, 5d). This demonstrates that in the SS model the decomposition of the surface  
 330 oxygen species is much faster than observed in the experiments. Both the HH (Figure 5e, 5f) and  
 331 the LB (Figure 5g, 5h) models showed consistent EO production across all delays measured, which  
 332 is closer to the experimental result, but do not show the peak production at 117 ms interval. A  
 333 small increase in EO production was seen in the LB model simulation when increasing the delay

334 from 20 to 50 ms, but this effect was much smaller than that measured experimentally. This shows  
335 that while the single-site models generally provide a better fit than the two-site models, they  
336 overpredict the stability of the surface oxide species and cannot recreate the complex relationship  
337 with surface oxide coverage and EO production observed experimentally.  
338

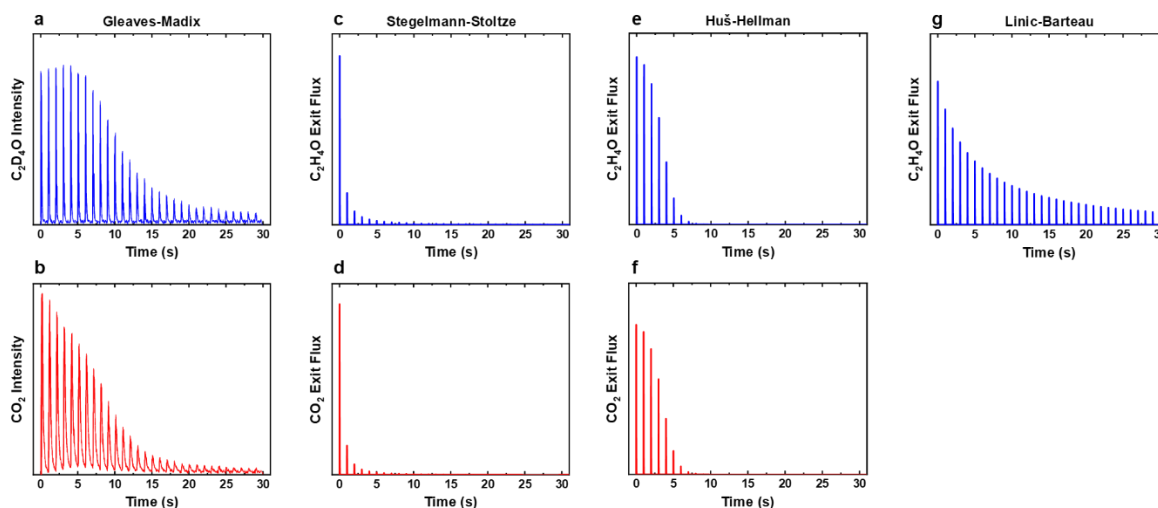


339  
340 **Figure 5.** (a-b) Experimental and (c-h) simulated ethylene oxide exit flux and ethylene oxide yield  
341 for pump-probe experiments with varied time interval between oxygen and ethylene pulses at 523  
342 K. Pump-probe time intervals were 20 ms (A), 50 ms (B), 72 ms (C), 117 ms (D), and 425 ms (E).  
343 The experimental results showed peak ethylene oxide production at 117 ms. (c,d) The SS model  
344 simulations showed peak ethylene oxide production at the shortest time interval, 20 ms, and  
345 subsequent decrease in production as the time interval between the two pulses increased. In both  
346 the HH and LB simulated results, ethylene oxide production was consistent across the varying time  
347 delays. Experimental data was adapted from ref.<sup>14</sup>  
348

349 **3.5 Multi-pulse Experiments.** In the oxidation-titration multi-pulse experiment the catalyst  
350 surface was first oxidised by applying 200 pulses of  $O_2$  and then the surface oxygen species were  
351 titrated off using pulses of ethylene.<sup>14</sup> This experiment provides insight into the activity and  
352 selectivity for EO production across the full range of surface oxide coverages, ranging from  
353 completely oxidised to completely reduced silver. Both the oxidation and titration were performed  
354 at 547 K. It was found in the experiment that EO production increased after the first few pulses,  
355 peaked, then decreased with increasing pulse number (Figure 6a). Conversely,  $CO_2$  production  
356 peaked in the first pulse and decayed with increasing pulse number (Figure 6b). This result  
357 indicated that a partially reduced surface is most active and selective for ethylene oxide production.  
358

359 None of the models were found to precisely recreate the experimentally observed trends in  
360 EO and  $CO_2$  production during the titration step. The SS model (Figure 6c and 6d) showed EO  
361 and  $CO_2$  production in the first few pulses, but production of both rapidly declined to zero  
362 afterwards, showing again that the rate of decomposition of the surface oxide is too fast. The HH

363 model (Figure 6e and 6f) was run with a 60% decreased surface area as the conversion was constant  
 364 at 100% for the first few pulses, obscuring the trends. After the first pulse there was then a rapid  
 365 decrease in production of the two products, however the selectivity to EO remained consistent  
 366 throughout, with the CO<sub>2</sub> responses matching the trend of the EO responses. The LB model (Figure  
 367 5g) showed a gradual decline in EO production during the simulation; however, peak production  
 368 was observed in the first pulse and the results did not display an increase and decrease in  
 369 production as observed experimentally. Similarly, it appears that the single-site models are able to  
 370 generally recreate the trends in activity observed experimentally, even at high surface oxide  
 371 coverages, but the finer kinetic features observed in the experiment are not recreated.  
 372



373  
 374 **Figure 6.** (a-b) Experimental and (c-g) simulated ethylene oxide and combustion product exit  
 375 fluxes for the titration experiment where ethylene was pulsed over the oxidised silver surface at  
 376 547 K. The HH model was run with 60% decreased surface area as the conversion of ethylene was  
 377 100% during the unmodified experiment. None of the models were found to recreate the  
 378 experimentally observed trends. Experimental data was adapted from ref.<sup>14</sup>  
 379

## 380 4. Discussion

381  
 382 **Table 2.** Summary of the simulated results and which models qualitatively reproduced trends  
 383 observed in the experiments. ✓ indicates experimental trend was recreated, ~ indicates  
 384 experimental trend was partially recreated, x indicates experimental trend was not recreated.

Model	Single-Pulse ( $\Delta T$ )			Pump-Probe		Multi-Pulse	
	C <sub>2</sub> H <sub>4</sub> Conversion	C <sub>2</sub> H <sub>4</sub> O Production	CO <sub>2</sub> Production	Ratio	Time Interval	C <sub>2</sub> H <sub>4</sub> O Production	CO <sub>2</sub> Production
SS	x	✓	~	~	x	x	x
HH	x	✓	~	✓	x	x	x
LB	x	✓	x	~	x	x	x

385  
386  
387  
388  
389  
390  
391  
392  
393  
394  
395  
396  
397  
398  
399  
400  
401  
402  
403  
404  
405  
406  
407

The simulations of the TAP experiments using the SS, HH, and LB models all failed to produce quantitative agreement with the experiments, but some experimental trends were recreated qualitatively (Table 2). In the single-pulse state defining experiments over metallic silver, the simulated production of EO and CO<sub>2</sub> followed the general trends of increasing with increasing temperature, but the simulations did not replicate the broadening of the CO<sub>2</sub> response seen at lower temperatures (Figure 3). Similarly, for the pump-probe experiments at varying O<sub>2</sub> to ethylene ratios, an increase in EO production was recorded with increasing O<sub>2</sub> to ethylene ratio, and the three models qualitatively recreated this trend (Figure 4), with the HH model matching most closely. However, when the ratio of O<sub>2</sub> to ethylene was fixed and the time delay was varied, a maximum of EO production was recorded at a delay time of 117 ms, whereas in the SS model the maxima was at the shortest time interval, and the HH and LB models showed no change with varying time delay (Figure 5). Finally, for the multi-pulse oxidation-titration experiment it was observed that the peak EO production does not occur in the first pulse but a few pulses in, with a gradual decline in production afterwards. None of the models recreated this trend in the simulations (Figure 6). It would appear that the LB and HH single-site models are most generally accurate for EO production, but do not properly capture the finer kinetic features observed as a function of surface oxide coverage, and struggle to reproduce the EO selectivity. The two-site model generally is limited by the rapid decomposition of the surface oxide. From the TAP experiments we identify the key feature being that the peak EO production was not in the first pulse during the multi-pulse ethylene titration, as other TAP-like experiments at atmospheric pressure have also observed this feature.<sup>26</sup>

408  
409  
410  
411  
412  
413  
414  
415  
416  
417  
418

During the multi-pulse titration experiments, the surface coverage of O\* is very high after the O<sub>2</sub> treatment, meaning that lateral interactions between O\* and other adsorbates become relevant. The HH model identified that significant lateral interactions between O\* and O\*, OME\*, and C<sub>2</sub>H<sub>4</sub>\* were present.<sup>4</sup> In an attempt to understand the role that lateral interactions play in the calculated activity and selectivity, the multi-pulse titration experiment was recreated where the rate constants were re-calculated based on the coverage of O\* after each pulse. The initial coverage was set to 0.4, as this was when the adsorption energy of O\* becomes positive over the Ag(111) surface.<sup>4</sup> The pairwise interactions between O\* and C<sub>2</sub>H<sub>4</sub> were found to be -9.65 kJ/mol (0.1 eV) and O\* and OME\* being 28.94 kJ/mol (0.3 eV). To approximate lateral interactions, the pairwise interaction between the adsorbates was assumed be a maximum at a coverage of 1, with a linear dependence on coverage. Step 1 was modified such that:

$$E_{a,rev}(\theta_{O^*}) = E_{a,rev}(0) - E_{pairwise}^{C_2H_4} \theta_{O^*} \quad (15)$$

419 where  $E_{a,rev}(\theta_{O^*})$  is the calculated activation barrier,  $E_{a,rev}(0)$  is the activation barrier at zero  
 420 coverage,  $E_{pairwise}^{C_2H_4}$  is the pairwise interaction between  $O^*$  and the adsorbate, and  $\theta_{O^*}$  is the  
 421 coverage of  $O^*$ . Step 5 was modified using the following expression:

$$E_{a,fwd}(\theta_{O^*}) = E_{a,fwd}(0) + E_{pairwise}^{OME} \theta_{O^*} \quad (16)$$

$$E_{a,rev}(\theta_{O^*}) = E_{a,rev}(0) + E_{pairwise}^{C_2H_4} \theta_{O^*} \quad (17)$$

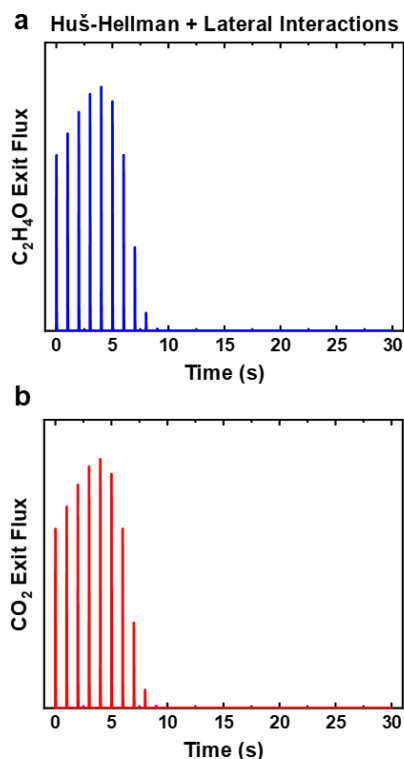
422 With step  $6_{fwd}$ ,  $7_{rev}$ , and  $8_{rev}$  also modified using equation 16. The coverages and rate constants for  
 423 the first 10 pulses are shown in Table 3.

424  
 425 **Table 3.** Calculated coverage dependent activation energies for the first 10 pulses of the multi-  
 426 pulse titration simulation for steps 1, 5, 6, 7 and 8 in the HH model<sup>4</sup> with lateral interactions. All  
 427 other parameters were kept consistent with the original experiment.

Pulse	Coverage	$E_a$ (kJ/mol)					
		$1_{fwd}$	$5_{fwd}$	$5_{rev}$	$6_{fwd}$	$7_{rev}$	$8_{rev}$
-	0	7.72	45.35	63.68	28.95	93.59	189.11
1	0.40	11.58	56.93	59.82	40.53	105.17	200.69
2	0.35	11.12	55.55	60.28	39.15	103.79	199.31
3	0.30	10.61	54.03	60.79	37.63	102.27	197.79
4	0.24	10.07	52.41	61.33	36.01	100.65	196.17
5	0.18	9.50	50.70	61.90	34.30	98.94	194.46
6	0.12	8.92	48.96	62.48	32.56	97.20	192.72
7	0.07	8.38	47.33	63.02	30.93	95.57	191.09
8	0.02	7.96	46.07	63.44	29.67	94.31	189.83
9	0.00	7.76	45.49	63.63	29.09	93.73	189.25
10	0.00	7.72	45.37	63.67	28.97	93.61	189.13

428



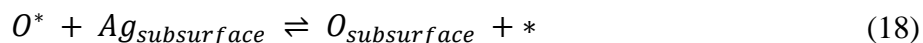


429  
 430 **Figure 7.** Simulated (a) ethylene oxide and (b) CO<sub>2</sub> exit flux for the multi-pulse titration  
 431 experiment over oxidised silver using the HH model with lateral interactions included. All other  
 432 parameters were kept consistent with the original experiment. Peak ethylene oxide production was  
 433 observed in pulse 5, with a rapid decrease in production observed afterwards. The same trend was  
 434 observed in the CO<sub>2</sub> (acetaldehyde) flux.

435  
 436 With the inclusion of lateral interactions in the HH model, the trend of increasing ethylene  
 437 oxide production for the first few pulses is observed (Figure 7) with the maximum ethylene oxide  
 438 production occurring on pulse 5. The exact same trend is observed in the CO<sub>2</sub> (acetaldehyde)  
 439 responses. While this is closer to the experimental response when lateral interactions are not  
 440 included (Figure 6), it still does not completely recreate the experimentally observed trends where  
 441 the CO<sub>2</sub> production peaks in the first pulse and then declines with increasing pulse number. This  
 442 means that the model is recreating the activity for EO production as a function of pulse number  
 443 but is not recreating the selectivity to EO correctly. This could be down to the fact that the model  
 444 only simulates acetaldehyde production, rather than CO<sub>2</sub>, and perhaps the rate limiting step for  
 445 CO<sub>2</sub> production is after the formation of acetaldehyde. However, it is important to note that  
 446 atmospheric pressure pulsed flow experiments observed a similar trend of constant selectivity.<sup>26</sup>  
 447 Further, this incorporation of lateral interactions in this model is flawed, as they are based on  
 448 pairwise interactions from Kinetic Monte Carlo simulations and the TAP simulations use a mean  
 449 field assumption. This demonstrates that single-site models, when accounting for lateral  
 450 interactions, can replicate more complex kinetic features observed during the experiments, which  
 451 can explain this models broad predictability for EO production across a wide range of materials.<sup>27</sup>

452 However, further refinement of the combustion pathway is required in order to precisely recreate  
453 the selectivity trends as a function of surface oxygen coverage.

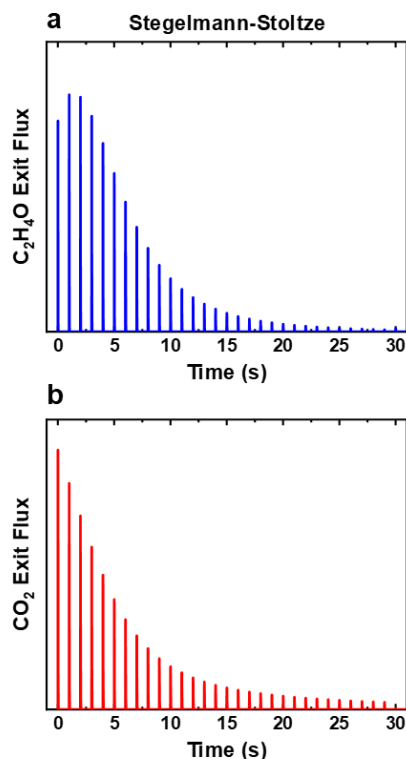
454  
455 For the SS model, based on the pump-probe with varied time interval and the multi-pulse  
456 titration simulations, the most significant error is related to the lifetime of the surface oxygen  
457 species. The rapid loss in EO production with increasing time (and pulse number) indicates that  
458 the surface oxygen species are desorbing quickly in this model. From the TAP experiments the  
459 half-life for the active oxygen species was estimated to be ~5 minutes at 523 K,<sup>14</sup> whereas in the  
460 pump-probe experiment with varying time intervals (Figure 5), the lifetime of the surface oxygen  
461 species in the SS model is significantly shorter as the production of EO is almost zero by 425 ms.  
462 In further work utilising the SS model, a type of subsurface oxygen was included.<sup>10</sup> However, it  
463 was found that this subsurface oxygen was not relevant to simulations under steady state  
464 conditions. These steps allow for the development of an “oxygen reservoir” below the surface that  
465 can supply oxygen to the surface, extending the lifetime of the active oxide species.



466 However, these steps could not be included in the SS model used in this work as the kinetic  
467 parameters were not reported and attempts to incorporate these steps with estimates were  
468 unsuccessful and generated unstable simulation results.

469  
470 Without including the extra steps in the model, one such method to recreate an oxygen  
471 reservoir is to run with the oxygen desorption steps (Table 1, Steps 1 reverse and 3 reverse) in the  
472 SS model turned off to remove oxygen decomposition. The objective of this change was to mimic  
473 the effect of having a reservoir of subsurface oxygen within the catalyst. When this was coupled  
474 with decreasing the pulse size by an order of magnitude ( $10^{16}$  molecules per pulse), we found that  
475 the SS model was able to recreate the experimental trend of peak EO production not being in the  
476 first pulse (Figure 8a). Additionally, peak production of CO<sub>2</sub> was observed in the first pulse in this  
477 simulation with production gradually decreasing throughout the experiment. Under these modified  
478 conditions we find the SS model provides an excellent recreation of the experiment (Figure 6a, 6b,  
479 8).

480



481  
 482 **Figure 8.** Simulated (a) ethylene oxide and (b) CO<sub>2</sub> exit flux for the titration experiment with  
 483 adjustments made to the Stegelmann-Stoltze (SS) model. Pulse size was decreased to  $1 \times 10^{16}$   
 484 molecules per pulse, and oxygen desorption steps (1 reverse and 3 reverse) were turned off. All  
 485 other parameters were kept consistent with the original experiment. Peak ethylene oxide  
 486 production was observed later than the first pulse, while peak production of CO<sub>2</sub> was observed in  
 487 the first pulse. These trends qualitatively match those observed in the experimental data (see Figure  
 488 4a, 4b).

489  
 490 Based on the simulation results, the SS model best recreates the experimental data as  
 491 measured by Gleaves and Madix, indicating that the underlying reaction network and rate  
 492 constants have some validity. However, the surface oxygen species appear to be less stable than  
 493 those measured experimentally. It would appear that for the less complex LB and HH models, the  
 494 single site model is sufficient to recreate some of the features observed in the experiments,  
 495 particularly with the inclusion of lateral interactions. However, for the SS model it would appear  
 496 the inclusion of the second “electrophilic oxygen” active site ( $O/O^*$ )<sup>5</sup> where oxygen is adsorbed  
 497 on top of the surface oxide ( $/O^*$ ) which reacts with ethylene to make the oxametallacycle alongside  
 498 a subsurface oxygen reservoir is important for recreating some of the finer features observed during  
 499 the multi-pulse experiment. Given the likelihood of multiple active phases existing on the catalyst  
 500 surface during ethylene epoxidation,<sup>9</sup> having multiple active sites in a model is important. The  
 501 broad applicability of this model far outside of its original training dataset indicates that the  
 502 proposed mechanism is a good candidate for ethylene epoxidation over metallic silver. However,

503 the lifetime of the oxygen species and the lack of quantitative agreement between the model and  
504 the experiment would indicate that some of the kinetic coefficients are poorly scaled.

505

#### 506 **4. Conclusions**

507

508 Simulations of the four experiments using the LB, HH, and SS models showed none of the  
509 models were able quantitatively recreate any of the observed experimental trends in EO production  
510 and ethylene combustion. Some qualitative agreement was found (Table 2), but none of the models  
511 recreated the experimentally observed trend of peak EO production and selectivity not being in the  
512 first pulse during the multi-pulse titration experiments over oxidised silver. By modifying the  
513 single-site HH model to include lateral interactions between adsorbates the trend in EO production  
514 was recreated, but the model was not able to recreate the trend in EO selectivity seen in the TAP  
515 experiments,<sup>14</sup> but matched that of atmospheric pressure pulsed flow experiments.<sup>26</sup> We find that  
516 the oxygen decomposition pathway in the SS model is incorrectly accounted for, leading to rapid  
517 decomposition of surface oxide species. We have related this to the omission of steps relating to a  
518 subsurface oxygen reservoir. With modifications to pulse size and the kinetics for oxygen  
519 decomposition set to zero, the SS model was the only of the three able to recreate both the  
520 production and selectivity to EO recorded during the multi-pulse titration experiments. The  
521 simulations suggest that the broad applicability of the SS model with its two active sites is a good  
522 candidate for the reaction mechanism for ethylene epoxidation over metallic silver, however some  
523 further refinement of the kinetic coefficients is desirable. Further, as the surface of silver is most  
524 likely oxidised under reaction conditions<sup>9</sup> some inclusion of a subsurface oxygen species is also  
525 recommended.

526

527 The general applicability of the single-site models means that their use for materials and  
528 reaction condition screening is still valid, but if we are to push beyond wide-ranging screening to  
529 more precise refinement of reaction conditions, more complex models are required. This work  
530 reinforces that even though the “ground truth” of ethylene epoxidation is very complicated,  
531 simpler, single site models can still recreate the majority of the trends in catalytic activity. Given  
532 the broad predictability of the HH model when lateral interactions are included,<sup>27</sup> and that the  
533 epoxidation of ethylene can occur on multiple different sites simultaneously,<sup>9</sup> it is most likely that  
534 all of these models contain some core truth within them, and that further transient experiments of  
535 ethylene epoxidation are required to identify the true reaction mechanism.

536

537 The original TAP experiments<sup>14</sup> that these simulations were designed to recreate were  
538 performed using an outdated methodology. In modern TAP setups the reactor is typically packed  
539 using a thin-layer of catalyst between two inert zones rather than filling the entire microreactor  
540 with catalyst.<sup>19</sup> Further, the precise diffusional characteristics of modern TAP systems means that  
541 the models are more applicable.<sup>12,20</sup> Future work replicating these experiments in a more modern  
542 TAP reactor would be highly desirable, and further exploration of varying reaction conditions and

543 temperatures could provide a framework for generating updated simulation parameters. More  
544 broadly, this approach of numerically recreating TAP experiments to validate kinetic models  
545 outside of their initial validation conditions can be generally applied to other heterogeneous  
546 catalytic systems.

547

## 548 **Supporting Information**

549

550 Included alongside this manuscript is a beta version of the MATLAB code SimTAP that was  
551 developed as part of this work, and the SimTAP input files for each experiment are also included.  
552 Please note that some simulations take a significant time to run.

553

## 554 **Acknowledgements**

555

556 C.R. gratefully acknowledges the Rowland Fellowship through the Rowland Institute at Harvard.  
557 C.R. and L.B. both acknowledge funding from the Program for Research in Science and  
558 Engineering (PRISE) summer programme. The computations in this paper were run on the FASRC  
559 Cannon cluster supported by the FAS Division of Science Research Computing Group at Harvard  
560 University.

561

## 562 **Author contributions**

563

564 Lilliana Brandao: Investigation, Validation, Data Curation, Writing – Original Draft  
565 Christian Reece: Conceptualisation, Methodology, Software, Writing – Review & Editing,  
566 Supervision, Funding Acquisition

567

568 L.B. Generated the SimTAP input files and performed the simulations and the data analysis. C.R.  
569 Wrote the SimTAP code and guided the research. All authors participated in frequent discussions  
570 and contributed significantly to writing the manuscript.

571

## 572 **Competing interests**

573

574 The authors declare no competing financial interest.

575

## 576 **References**

577

578 (1) AgileIntel Research (ChemIntel360). *Market value of ethylene oxide worldwide from 2015*  
579 *to 2022, with a forecast for 2023 to 2030*. Statista.  
580 <https://www.statista.com/statistics/1244434/global-market-value-ethylene-oxide/> (accessed  
581 2023-08-02).

- 582 (2) Pu, T.; Tian, H.; Ford, M. E.; Rangarajan, S.; Wachs, I. E. Overview of Selective Oxidation  
583 of Ethylene to Ethylene Oxide by Ag Catalysts. *ACS Catalysis* **2019**, 10727–10750.  
584 <https://doi.org/10.1021/acscatal.9b03443>.
- 585 (3) Linic, S.; Barteau, M. A. Construction of a Reaction Coordinate and a Microkinetic Model  
586 for Ethylene Epoxidation on Silver from DFT Calculations and Surface Science  
587 Experiments. *Journal of Catalysis* **2003**, 214 (2), 200–212. [https://doi.org/10.1016/S0021-](https://doi.org/10.1016/S0021-9517(02)00156-2)  
588 [9517\(02\)00156-2](https://doi.org/10.1016/S0021-9517(02)00156-2).
- 589 (4) Huš, M.; Hellman, A. Ethylene Epoxidation on Ag(100), Ag(110), and Ag(111): A Joint Ab  
590 Initio and Kinetic Monte Carlo Study and Comparison with Experiments. *ACS Catalysis*  
591 **2019**, 9 (2), 1183–1196. <https://doi.org/10.1021/acscatal.8b04512>.
- 592 (5) Stegelmann, C.; Schiødt, N. C.; Campbell, C. T.; Stoltze, P. Microkinetic Modeling of  
593 Ethylene Oxidation over Silver. *Journal of Catalysis* **2004**, 221 (2), 630–649.  
594 <https://doi.org/10.1016/j.jcat.2003.10.004>.
- 595 (6) Pu, T.; Setiawan, A.; Mosevitzky Lis, B.; Zhu, M.; Ford, M. E.; Rangarajan, S.; Wachs, I.  
596 E. Nature and Reactivity of Oxygen Species on/in Silver Catalysts during Ethylene  
597 Oxidation. *ACS Catalysis* **2022**, 12 (8), 4375–4381.  
598 <https://doi.org/10.1021/acscatal.1c05939>.
- 599 (7) Jones, T. E.; Wyrwich, R.; Böcklein, S.; Carbonio, E. A.; Greiner, M. T.; Klyushin, A. Y.;  
600 Moritz, W.; Locatelli, A.; Menteş, T. O.; Niño, M. A.; Knop-Gericke, A.; Schlögl, R.;  
601 Günther, S.; Wintterlin, J.; Piccinin, S. The Selective Species in Ethylene Epoxidation on  
602 Silver. *ACS Catalysis* **2018**, 8 (5), 3844–3852. <https://doi.org/10.1021/acscatal.8b00660>.
- 603 (8) Lockemeyer, J. R.; Lohr, T. L. Ethylene Oxide Catalysis Under Commercial Conditions –  
604 A Guide for Researchers. *ChemCatChem* **2023**, 15 (13), e202201511.  
605 <https://doi.org/10.1002/cctc.202201511>.
- 606 (9) Liu, J.-X.; Lu, S.; Ann, S.-B.; Linic, S. Mechanisms of Ethylene Epoxidation over Silver  
607 from Machine Learning-Accelerated First-Principles Modeling and Microkinetic  
608 Simulations. *ACS Catal.* **2023**, 13 (13), 8955–8962.  
609 <https://doi.org/10.1021/acscatal.3c00410>.
- 610 (10) Stegelmann, C.; Stoltze, P. Microkinetic Analysis of Transient Ethylene Oxidation  
611 Experiments on Silver. *Journal of Catalysis* **2004**, 226 (1), 129–137.  
612 <https://doi.org/10.1016/j.jcat.2004.03.047>.
- 613 (11) Campbell, C. T. The Degree of Rate Control: A Powerful Tool for Catalysis Research. *ACS*  
614 *Catal.* **2017**, 7 (4), 2770–2779. <https://doi.org/10.1021/acscatal.7b00115>.
- 615 (12) Gleaves, J. T.; Yablonskii, G. S.; Phanawadee, P.; Schuurman, Y. TAP-2: An Interrogative  
616 Kinetics Approach. *Appl. Catal. A-Gen.* **1997**, 160 (1), 55–88.  
617 [https://doi.org/10.1016/S0926-860X\(97\)00124-5](https://doi.org/10.1016/S0926-860X(97)00124-5).
- 618 (13) Morgan, K.; Maguire, N.; Fushimi, R.; Gleaves, J. T.; Goguet, A.; Harold, M. P.;  
619 Kondratenko, E. V.; Menon, U.; Schuurman, Y.; Yablonsky, G. S. Forty Years of Temporal  
620 Analysis of Products. *Catal. Sci. Technol.* **2017**, 7 (12), 2416–2439.  
621 <https://doi.org/10.1039/C7CY00678K>.
- 622 (14) Gleaves, J. T.; Sault, A. G.; Madix, R. J.; Ebner, J. R. Ethylene Oxidation on Silver  
623 Powder: A Tap Reactor Study. *Journal of Catalysis* **1990**, 121 (1), 202–218.  
624 [https://doi.org/10.1016/0021-9517\(90\)90230-H](https://doi.org/10.1016/0021-9517(90)90230-H).
- 625 (15) Roelant, R. Mathematical Determination of Reaction Networks from Transient Kinetic  
626 Experiments, Universitet Ghent, 2011.

- 627 (16) Reece, C.; Redekop, E. A.; Karakalos, S.; Friend, C. M.; Madix, R. J. Crossing the Great  
628 Divide between Single-Crystal Reactivity and Actual Catalyst Selectivity with Pressure  
629 Transients. *Nature Catalysis* **2018**, *1* (11). <https://doi.org/10.1038/s41929-018-0167-5>.
- 630 (17) Yonge, A.; Kunz, M. R.; Batchu, R.; Fang, Z.; Issac, T.; Fushimi, R.; Medford, A. J.  
631 TAPsolver: A Python Package for the Simulation and Analysis of TAP Reactor  
632 Experiments. *Chemical Engineering Journal* **2021**, *420* (P1).  
633 <https://doi.org/10.1016/j.cej.2021.129377>.
- 634 (18) Constales, D.; Yablonsky, G. S.; Marin, G. B.; Gleaves, J. T. Multi-Zone TAP-Reactors  
635 Theory and Application: I. The Global Transfer Matrix Equation. *Chem. Eng. Sci.* **2001**, *56*  
636 (1), 133–149. [https://doi.org/10.1016/S0009-2509\(00\)00216-5](https://doi.org/10.1016/S0009-2509(00)00216-5).
- 637 (19) Shekhtman, S. O.; Yablonsky, G. S.; Chen, S.; Gleaves, J. T. Thin-Zone TAP-Reactor -  
638 Theory and Application. *Chem. Eng. Sci.* **1999**, *54* (20), 4371–4378.  
639 [https://doi.org/10.1016/S0009-2509\(98\)00534-X](https://doi.org/10.1016/S0009-2509(98)00534-X).
- 640 (20) Brandão, L.; High, E. A.; Kim, T.-S.; Reece, C. Simplifying the Temporal Analysis of  
641 Products Reactor. *Chem. Eng. J.* **2023**, *478*, 147489.  
642 <https://doi.org/10.1016/j.cej.2023.147489>.
- 643 (21) Constales, D.; Yablonsky, G. S.; Marin, G. B.; Gleaves, J. T. Multi-Zone TAP-Reactors  
644 Theory and Application. III Multi-Response Theory and Criteria of Instantaneousness.  
645 *Chemical Engineering Science* **2004**, *59* (17), 3725–3736.  
646 <https://doi.org/10.1016/j.ces.2004.05.023>.
- 647 (22) Redekop, E. A.; Yablonsky, G. S.; Constales, D.; Ramachandran, P. A.; Gleaves, J. T.;  
648 Marin, G. B. Elucidating Complex Catalytic Mechanisms Based on Transient Pulse-  
649 Response Kinetic Data. *Chemical Engineering Science* **2014**, *110*, 20–30.  
650 <https://doi.org/10.1016/j.ces.2013.11.050>.
- 651 (23) Lukaski, A. C.; Barteau, M. A. Investigation of Ethylene Oxide on Clean and Oxygen-  
652 Covered Ag(110) Surfaces. *Catal Lett* **2009**, *128* (1–2), 9–17.  
653 <https://doi.org/10.1007/s10562-008-9802-0>.
- 654 (24) Schuurman, Y. Assessment of Kinetic Modeling Procedures of TAP Experiments. *Catalysis*  
655 *Today* **2007**, *121* (3–4), 187–196. <https://doi.org/10.1016/j.cattod.2006.06.046>.
- 656 (25) Dumesic, J. A.; Rudd, D. F.; Aparicio, L. M.; Rekoske, J. E.; Treviño, A. A. *The*  
657 *Microkinetics of Heterogeneous Catalysis*; American Chemical Society, 1993.
- 658 (26) Scharfenberg, L.; Horn, R. Temporal Analysis of Products Experiments at Atmospheric  
659 Pressure: The Epoxidation of Ethylene on Silver. *Chemie-Ingenieur-Technik* **2017**, *89* (10),  
660 1350–1359. <https://doi.org/10.1002/cite.201700071>.
- 661 (27) Huš, M.; Grilc, M.; Teržan, J.; Gyergyek, S.; Likozar, B.; Hellman, A. Going Beyond  
662 Silver in Ethylene Epoxidation with First-Principles Catalyst Screening. *Angew Chem Int*  
663 *Ed* **2023**, *62* (31), e202305804. <https://doi.org/10.1002/anie.202305804>.
- 664